1 SCIENTIFIC HIGHLIGHT OF THE MONTH

Many-Body van der Waals Interactions in Biology, Chemistry, and Physics

Robert A. DiStasio Jr.[1], Vivekanand V. Gobre[2], and Alexandre Tkatchenko[2]

[1] *Department of Chemistry, Princeton University, Princeton, NJ 08544, USA*
[2] *Fritz-Haber-Institut der Max-Planck-Gesellschaft, Faradayweg 4-6, 14195, Berlin, Germany*

tkatchenko@fhi-berlin.mpg.de, distasio@princeton.edu

Abstract

This work presents increasing evidence that many-body van der Waals (vdW) dispersion interactions play a crucial role in the structure, stability, and function of a wide variety of systems in biology, chemistry, and physics. We start by deriving both pairwise and many-body interatomic methods for computing the dispersion energy by considering a system of coupled quantum harmonic oscillators (QHO) within the random-phase approximation (RPA). The resulting many-body dispersion (MBD) method contains two types of energetic contributions that arise from beyond-pairwise (non-additive) interactions and electrodynamic response screening. Applications are presented that address benchmark databases of intermolecular interactions, the stability of extended and globular conformations of alanine tetrapeptide, binding in the "buckyball catcher" supramolecular host–guest complex, and cohesion in oligoacene molecular crystals. We find that the beyond-pairwise vdW interactions and electrodynamic screening are shown to play a quantitative, and sometimes even qualitative, role in describing the properties considered herein. This highlight is concluded with a discussion of the challenges that remain in the future development of reliable (accurate and efficient) methods for treating many-body vdW interactions in complex materials.

1 Introduction

The relevance of van der Waals (vdW) interactions in the structure, stability, and function of molecules and materials can hardly be overemphasized [1, 2, 3, 4, 5]. Ubiquitous in nature, vdW interactions act at distances from just a few Ångström to several nanometers, with recent experiments suggesting that vdW forces can even be significantly longer-ranged [6, 7]. VdW interactions are largely responsible for the formation of the gas-phase benzene dimer at low temperatures, the stabilization required for the formation of molecular crystals, and the binding of molecules to proteins and DNA inside living cells. In addition, vdW interactions play a central role in the fields of supramolecular chemistry and nano-materials, in which non-covalent binding is essential for structure and functionality.

In order to enable rational predictions and design of molecular and condensed-matter materials, including interfaces between them, a reliable first-principles method is required that can describe vdW interactions both accurately and efficiently. However, an accurate description of vdW interactions is extremely challenging, since the vdW dispersion energy arises from the correlated motion of electrons and must be described by quantum mechanics. The rapid increase in computational power coupled with recent advances in the development of theoretical models for describing vdW interactions have allowed us to achieve so-called "chemical accuracy" for binding between small organic molecules. However, the lack of accurate and efficient methods for treating large and complex systems hinders truly quantitative predictions of the properties and functions of technologically and biologically relevant materials.

Many encouraging approaches have been proposed in recent years for approximately including long-range pairwise dispersion interactions in density-functional theory (DFT) [8, 9, 10, 11, 12, 13, 14, 15, 16, 17]. Despite significant progress in the field of modeling vdW interactions, many questions still remain and further development is required before a universally applicable method emerges. For example, pairwise interatomic vdW methods are frequently employed to describe organic molecules adsorbed on inorganic surfaces [18, 19, 20, 21], ignoring the relatively strong electrodynamic response screening present within bulk materials. On the other hand, the popular non-local vdW-DF functionals [22, 23, 24] utilize a homogeneous dielectric approximation for the polarizability, which is not expected to be accurate for molecules. Despite this fact, interaction energies between small organic molecules computed with such functionals turn out to be reasonably accurate. Understanding the physical reasons as to why these different approaches "yield good results" outside of their expected domain of applicability is important for the development of more robust approximations.

Interatomic pairwise dispersion approaches based on the standard C_6/R^6 summation formula were popularized by the DFT-D method of Grimme [10] and are now among the most widely used methods [9, 12, 13] for including the dispersion energy in DFT. Despite their simplicity, these pairwise models provide remarkable accuracy when applied to small molecular systems, especially when accurate dispersion coefficients (C_6) are employed for atoms in molecules [25, 26]. Only recently have efforts been focused on going beyond the pairwise treatment of vdW contributions, for example, the importance of the non-additive three-body interatomic Axilrod-Teller-Muto term [27, 28, 29] was assessed, as well as the role of non-local screening in solids [30] and molecules adsorbed on surfaces [31]. Furthermore, an efficient and accurate interatomic many-body dispersion (MBD) approach has been recently proposed [32], which demonstrated that a many-body description of vdW interactions is essential for extended molecules and molecular solids, and the influence of many-body interactions can already become significant when considering the binding between relatively small organic molecules [32, 33].

In this highlight, we present a derivation of the pairwise and many-body interatomic dispersion energy for an arbitrary collection of isotropic polarizable dipoles from the adiabatic connection fluctuation-dissipation (ACFD) formula, which is an exact expression for the exchange-correlation energy. We distinguish and discuss two types of interatomic many-body contributions to the dispersion energy, which stem from beyond-pairwise non-additive interactions and self-consistent electrodynamic response screening. By using the ACFD formula we gain a deeper understanding of the approximations made in interatomic approaches, in particular the

DFT+MBD method [32], providing a powerful formalism for further development of accurate and efficient methods for the calculation of the vdW dispersion energy.

Applications of the DFT+MBD method are presented for a variety of systems, including benchmark databases of intermolecular interactions, the stability of extended and globular conformations of alanine tetrapeptide, the binding in the "buckyball catcher" supramolecular host–guest complex, and the cohesive energy of several oligoacene molecular crystals. For all of these cases, the role of the beyond-pairwise non-additive vdW interactions and electrodynamic screening captured at the DFT+MBD level of theory is critically assessed and shown to contribute in a quantitative, and sometimes even qualitative, fashion. We conclude this highlight with a discussion of the challenges that remain in the future development of accurate and efficient methods for treating many-body vdW interactions in materials of increasing complexity.

As the modeling of vdW interactions is currently a very active field of research, it is impossible to cover all of the important developments in this highlight. For more information, we refer interested readers to the recent Ψ_k highlight by Dobson and Gould, which discusses several different approaches for computing dispersion interactions [34]; to the review by Klimes and Michaelides on dispersion methods within DFT [35]; and to the webpage for the recent vdW@CECAM workshop that brought together many of the key players in the development and application of vdW-inclusive first-principles methods [36].

2 Theory

The adiabatic connection fluctuation-dissipation (ACFD) theorem provides a general and exact expression for the exchange-correlation energy [37, 38], thereby allowing for the calculation of the dispersion energy in a seamless and accurate fashion which naturally incorporates higher-order many-body effects. In this section, we explore the use of the ACFD theoretical framework as a basis for the understanding and future development of interatomic pairwise and many-body dispersion methods. Beginning with a brief derivation of the ACFD correlation energy within the random-phase approximation (RPA), we then consider the ACFD-RPA correlation energy for a system of quantum harmonic oscillators (QHO) interacting *via* the dipole-dipole potential. We derive the well-known C_6/R^6 interatomic pairwise summation formula from the second-order expansion of the ACFD-RPA correlation energy for an arbitrary collection of N QHOs, each of which is characterized by an isotropic frequency-dependent point dipole polarizability. We then extend our model to account for spatially distributed dipole polarizabilities and derive modified range-separated Coulomb and dipole–dipole interaction potentials that attenuate the short-range interactions. The self-consistent screening (SCS) method is introduced which allows us to obtain accurate screened atomic polarizabilities that are subsequently utilized as input for the MBD method to calculate the fully screened many-body dispersion energy. Finally, the coupling of the MBD method with standard DFT functionals (DFT+MBD method) is achieved by employing a range-separated Coulomb potential, and allows us to treat the full range of exchange and correlation effects.

2.1 The ACFD-RPA Correlation Energy Expression

For a system of nuclei and electrons, the ACFD theorem provides us with an exact expression for the exchange-correlation energy in terms of the density-density response function $\chi(\mathbf{r}, \mathbf{r}', \mathrm{i}\omega)$ [37, 38], which measures the electronic response of the system at a point $\mathbf{r}$ due to a frequency-dependent electric field perturbation at a point $\mathbf{r}'$. Since the focus of this work is on dispersion, which is a quantum mechanical phenomena due to the instantaneous (dynamical) correlation between electrons, we write the ACFD formula for the correlation energy as (Hartree atomic units are assumed throughout):

$$E_c = -\frac{1}{2\pi}\int_0^\infty d\omega \int_0^1 d\lambda\, \mathbf{Tr}[(\chi_\lambda(\mathbf{r}, \mathbf{r}', \mathrm{i}\omega) - \chi_0(\mathbf{r}, \mathbf{r}', \mathrm{i}\omega))v(\mathbf{r}, \mathbf{r}')]. \tag{1}$$

In this expression, $\chi_0(\mathbf{r}, \mathbf{r}', \mathrm{i}\omega)$ is the bare or non-interacting particle response function, which can be computed given a set of single-particle orbitals $\{\phi_i\}$ with corresponding energies $\{\epsilon_i\}$ and occupation numbers $\{f_i\}$ [39, 40] as

$$\chi_0(\mathbf{r}, \mathbf{r}', \mathrm{i}\omega) = \sum_{ij}(f_i - f_j)\frac{\phi_i^*(\mathbf{r})\phi_i(\mathbf{r}')\phi_j^*(\mathbf{r}')\phi_j(\mathbf{r})}{\epsilon_i - \epsilon_j + \mathrm{i}\omega}, \tag{2}$$

and $\chi_\lambda(\mathbf{r}, \mathbf{r}', \mathrm{i}\omega)$ is the interacting response function at Coulomb coupling strength λ, $v(\mathbf{r}, \mathbf{r}') = |\mathbf{r} - \mathbf{r}'|^{-1}$ is the Coulomb potential, and $\mathbf{Tr}$ denotes the trace operator (or six-dimensional integration) over the spatial variables $\mathbf{r}$ and $\mathbf{r}'$. The interacting response function, χ_λ, is defined self-consistently *via* the Dyson-like screening equation, $\chi_\lambda = \chi_0 + \chi_0(\lambda v + f_\lambda^{xc})\chi_\lambda$, which contains $f_\lambda^{xc}(\mathbf{r}, \mathbf{r}', \mathrm{i}\omega)$, the exchange-correlation kernel, which must be approximated in practice.

Within the ACFD formalism, the *adiabatic connection* between a reference non-interacting system (defined at $\lambda = 0$) and the fully interacting system (with $\lambda = 1$), yields the correlation energy of the system of interest, which contains the many-body dispersion energy as well as other electron correlation effects. This is most easily facilitated by neglecting the explicit dependence of f_λ^{xc} on the coupling constant, which allows for analytic integration over λ in the ACFD correlation energy expression in Eq. (1), and forms the basis for the most widely employed approximation for f_λ^{xc}, namely the random-phase approximation (RPA) [41, 42]. In what follows, we utilize the RPA, wherein $f_\lambda^{xc} = 0$, which has been shown to yield reliable results for a wide variety of molecules and extended systems [43, 44, 45, 46, 47, 48, 49, 50, 51, 52, 53, 54, 55, 56, 57, 58]. In the RPA, the ACFD correlation energy expression can be written as a power series expansion in $\chi_0 v$, following elimination of χ_λ using the Dyson equation and analytical integration over λ (*c.f.* Eq. (1)) [59, 60]:

$$E_{c,\mathrm{RPA}} = -\frac{1}{2\pi}\int_0^\infty d\omega \sum_{n=2}^{\infty}\frac{1}{n}\mathbf{Tr}[(\chi_0(\mathbf{r}, \mathbf{r}', \mathrm{i}\omega)v(\mathbf{r}, \mathbf{r}'))^n]. \tag{3}$$

For a more detailed review of the RPA approach for computing the correlation energy, see Refs. [34, 58, 61] and references therein.

2.2 Derivation of the Long-Range Interatomic Pairwise Dispersion Energy

We now apply the ACFD-RPA approach to compute the correlation energy for a collection of interacting QHOs representing the atoms in a molecular system of interest. In doing so, we will

first derive the standard C_6/R^6 interatomic pairwise summation formula for a system of two QHOs as the second-order expansion of the ACFD-RPA correlation energy within the dipole approximation. We will then demonstrate the validity of this formula for an arbitrary collection of N QHOs, providing a rigorous quantum mechanical derivation of the long-range interatomic pairwise summation formula for the dispersion energy.

In what follows, each atom p in a molecular system of interest will be mapped onto a single QHO characterized by a position vector $\mathbf{R_p} = \{x_p, y_p, z_p\}$ and a corresponding frequency-dependent dipole polarizability,

$$\alpha_p(\mathrm{i}\omega) = \frac{\alpha_p^0}{1 + (\omega/\omega_p)^2}, \tag{4}$$

which is completely determined by an isotropic static dipole polarizability, $\alpha_p^0 \equiv \alpha_p(0)$, and an effective (characteristic) excitation frequency, ω_p. To evaluate the ACFD-RPA correlation energy expression in Eq. (3), we first need the bare or non-interacting response function for the collection of QHOs, which is assembled as a direct sum over the individual QHO response functions, $\chi_0^p(\mathbf{r}, \mathbf{r'}, \mathrm{i}\omega)$, which take on the following matrix form for a QHO located at $\mathbf{R_p}$ and characterized by an isotropic point dipole polarizability [61]:

$$\chi_0^p(\mathbf{r}, \mathbf{r'}, \mathrm{i}\omega) = -\alpha_p(\mathrm{i}\omega)\nabla_{\mathbf{r}}\delta^3(\mathbf{r} - \mathbf{R_p}) \otimes \nabla_{\mathbf{r'}}\delta^3(\mathbf{r'} - \mathbf{R_p}), \tag{5}$$

where $\delta^3(\mathbf{r}-\mathbf{r'})$ is the three-dimensional Dirac delta function, and $\otimes$ is the tensor (outer) product. For the moment, we assume that the QHOs are separated by a sufficiently large distance, allowing us to use the bare dipole-dipole interaction potential to describe the interoscillator couplings, a condition that will be relaxed when the general case is considered in the next section. This dipole-dipole interaction potential between oscillators p and q is straightforwardly obtained from the bare Coulomb potential, $v_{pq} = |\mathbf{R_p} - \mathbf{R_q}|^{-1}$, *via*

$$\mathfrak{T}_{pq} = \begin{cases} \nabla_{\mathbf{R_p}} \otimes \nabla_{\mathbf{R_q}} v_{pq} & \text{if } p \neq q \\ 0 & \text{if } p = q \end{cases} \tag{6}$$

and is therefore a 3×3 second-rank tensor with components given by

$$\mathfrak{T}_{pq}^{ab} = -\frac{3R_aR_b - R_{pq}^2\delta_{ab}}{R_{pq}^5}, \tag{7}$$

in which a and b represent the coordinates $\{x, y, z\}$ in the Cartesian reference frame, R_a and R_b are the respective components of the interoscillator distance R_{pq}, and δ_{ab} is the standard Kronecker delta function. With the individual QHO response functions and the dipole-dipole interaction tensor as defined above, we now consider the quantity $\chi_0 v$ in the ACFD-RPA correlation energy expression in Eq. (3), which can be represented in matrix form as the product AT. Here, A is a diagonal $3N \times 3N$ matrix with $-\alpha_p(\mathrm{i}\omega)$ values on the 3×3 diagonal atomic subblocks, representing the bare or non-interacting response function for the collection of N QHOs. The dipole-dipole interaction matrix T is a $3N \times 3N$ matrix comprised of the 3×3 blocks of the $\mathfrak{T}_{pq}$ tensor defined in Eqs. (6) and (7).

For a system composed of two QHOs separated by a distance $R = |\mathbf{R_p} - \mathbf{R_q}|$ along the z-axis and characterized by the isotropic point dipole polarizabilities $\alpha_p(\mathrm{i}\omega)$ and $\alpha_q(\mathrm{i}\omega)$, the AT matrix

takes on the following form:

$$\chi_0 v \Leftrightarrow AT = \begin{pmatrix} 0 & 0 & 0 & -\frac{\alpha_p(\mathrm{i}\omega)}{R^3} & 0 & 0 \\ 0 & 0 & 0 & 0 & -\frac{\alpha_p(\mathrm{i}\omega)}{R^3} & 0 \\ 0 & 0 & 0 & 0 & 0 & \frac{2\alpha_p(\mathrm{i}\omega)}{R^3} \\ -\frac{\alpha_q(\mathrm{i}\omega)}{R^3} & 0 & 0 & 0 & 0 & 0 \\ 0 & -\frac{\alpha_q(\mathrm{i}\omega)}{R^3} & 0 & 0 & 0 & 0 \\ 0 & 0 & \frac{2\alpha_q(\mathrm{i}\omega)}{R^3} & 0 & 0 & 0 \end{pmatrix}. \tag{8}$$

With the above matrix as input, the second-order ($n = 2$) term of the ACFD-RPA correlation energy expression in Eq. (3) yields

$$E_{c,\mathrm{RPA}}^{(2)} = -\frac{1}{2\pi}\int_0^\infty d\omega\, \alpha_p(\mathrm{i}\omega)\alpha_q(\mathrm{i}\omega)\mathbf{Tr}[(\mathfrak{T}_{pq})^2] = -\frac{C_6^{pq}}{R^6}, \tag{9}$$

where we have used the fact that $\mathbf{Tr}[(\mathfrak{T}_{pq})^2] = 6/R_{pq}^6$ and the Casimir-Polder integral

$$C_6^{pq} = \frac{3}{\pi}\int_0^\infty d\omega\, \alpha_p(\mathrm{i}\omega)\alpha_q(\mathrm{i}\omega) \tag{10}$$

to determine the C_6^{pq} dispersion coefficient from the corresponding pair of frequency-dependent dipole polarizabilities. The above equation is of course the familiar expression for the long-range dispersion interaction between two spherical atoms.

To demonstrate the validity of this formula for an arbitrary collection of N QHOs, one needs to consider the action of the spatial trace operator in Eq. (3) on the general $3N \times 3N$ AT matrix. As seen above, the second-order term in the ACFD-RPA correlation energy expansion requires the trace of the square of the AT matrix, for which the p-th diagonal element is simply the scalar product between the corresponding p-th column and p-th row of AT. As such, the overall trace corresponds to an accumulated sum of the diagonal elements contained in the smaller $(\mathfrak{T}_{pq})^2$ subblocks $\forall\, p, q$, each weighted by the product $\alpha_p(\mathrm{i}\omega)\alpha_q(\mathrm{i}\omega)$. Since $\mathbf{Tr}[(\mathfrak{T}_{pq})^2] = 6/R_{pq}^6$ for any subblock $\mathfrak{T}_{pq}$, regardless of the geometry of the oscillator assembly, the second-order expansion of Eq. (3) reduces to

$$E_{c,\mathrm{RPA}}^{(2)} = -\frac{1}{2}\sum_{pq}\frac{C_6^{pq}}{R_{pq}^6}, \tag{11}$$

following the repeated use of the Casimir-Polder identity in Eq. (10) to determine the set of interoscillator dispersion coefficients. The reader will notice that this expression is nothing more than the standard interatomic pairwise summation formula utilized by methods such as DFT-D to compute the dispersion energy corresponding to a collection of N atoms.

Although the second-order expansion of the ACFD-RPA correlation energy in Eq. (3) yields the familiar interatomic pairwise expression for the dispersion energy given by Eq. (11), the former equation is more general and provides us with a powerful formalism for the further development of highly accurate and efficient methods for computing the dispersion energy in molecular systems of interest. For one, the ACFD-RPA correlation energy expression allows for the explicit utilization of the tensor form of the frequency-dependent dipole polarizability, enabling a fully anisotropic treatment of the dispersion energy. In this regard, anisotropy in the polarizability has been found to play a non-negligible role in the accurate description of intermolecular dispersion interactions [62, 63]. In the next two sections, we extend our above

treatment by considering QHOs characterized by spatially distributed (instead of point) dipole polarizabilities and describe a method for capturing the anisotropy in the frequency-dependent dipole polarizability based on the solution of the self-consistent Dyson-like screening equation of classical electrodynamics. Secondly, the use of the untruncated ACFD-RPA correlation energy expression allows for the explicit inclusion of the higher-order ($n > 2$) energetic contributions that arise naturally in the power series expansion of $\chi_0 v$. These terms include two distinct energetic contributions: the beyond-pairwise (non-additive) many-body interactions (to N^{th} order) and the higher-order electrodynamic response screening (to *infinite* order). The first example of the beyond-pairwise many-body interactions is captured in the third-order expansion of the ACFD-RPA correlation energy (for a system with $N \geq 3$), which is the so-called Axilrod-Teller-Muto triple-dipole term [64]. The higher-order response screening is most easily illustrated by considering a system composed of two QHOs p and q and expanding Eq. (3):

$$E_{c,\text{RPA}} = -\frac{1}{2\pi}\int_0^\infty d\omega \left(\frac{6\,\alpha_p(\mathrm{i}\omega)\alpha_q(\mathrm{i}\omega)}{R_{pq}^6} + \frac{9\,\alpha_p^2(\mathrm{i}\omega)\alpha_q^2(\mathrm{i}\omega)}{R_{pq}^{12}} + \ldots \right), \tag{12}$$

in which the second-order term corresponds to the "standard" C_6/R^6 pairwise dispersion interaction and the higher-order terms (which only survive with even powers of n) correspond to the electrodynamic screening of the polarizability of atom p by the presence of atom q and vice versa. In section 2.5, we again extend our above treatment and describe a method that accurately and efficiently accounts for both beyond-pairwise non-additive many-body and higher-order electrodynamic response screening contributions to the dispersion energy for an arbitrary system of N QHOs.

2.3 Extension to Spatially Distributed Dipole Polarizabilities

Correlation energy calculations carried out using the ACFD-RPA formula typically employ the bare response function, χ_0, computed using the set of occupied and virtual (unoccupied) single-particle orbitals obtained from self-consistent Hartree-Fock, semi-local DFT, or hybrid DFT calculations *via* Eq. (2). When constructed in this fashion, χ_0 accounts for orbital product (overlap) effects between the single-particle occupied and virtual states and is therefore a relatively delocalized object. On the other hand, when χ_0 is completely localized, its real-space matrix representation is diagonal in form, reflecting the fact that orbital product (overlap) effects have been neglected in the bare response function—this was the case for the A matrix corresponding to the collection of QHOs considered in the previous section. In this limit of fluctuating point dipoles, the interaction between QHOs diverges when the interoscillator distances become relatively close.

In the previous section, we assumed that the QHOs were separated by a sufficiently large distance to allow us to describe the interactions between them using the bare dipole-dipole potential, a condition that will now be relaxed in order to consider the general case, in which QHOs can be separated by typical chemical bond distances. The most straightforward way to avoid the near-field divergence is to incorporate orbital product (overlap) effects for the set of QHOs through a modification of the interaction potential at short interoscillator distances. Therefore, instead of using the bare Coulomb potential to derive the dipole-dipole interaction tensor, we

will utilize a modified Coulomb potential that (*i*) accounts for orbital product (overlap) effects at short interoscillator distances and (*ii*) becomes equivalent to the bare Coulomb potential in the long-range. This range-separated Coulomb potential can actually be rigorously derived from first principles by utilizing fundamental quantum mechanics, *i.e.*, the solutions of the Schrödinger equation for the QHO. In order to proceed, we first note that the ground state QHO wavefunction, $\psi_0^{\text{QHO}}(\mathbf{r})$, is a spherical Gaussian function and hence the corresponding ground state QHO charge density is also a spherical Gaussian function by the Gaussian product theorem, *i.e.*,

$$n_0^{\text{QHO}}(\mathbf{r}) = |\psi_0^{\text{QHO}}(\mathbf{r})|^2 = \frac{\exp[-\text{r}^2/2\sigma^2]}{\pi^{3/2}\sigma^3}, \tag{13}$$

in which σ represents the width or spread of the Gaussian. The corresponding Coulomb interaction between two spherical Gaussian charge distributions associated with oscillators p and q can then be derived as [65]

$$\overline{v}_{pq} = \frac{\text{erf}[R_{pq}/\sigma_{pq}]}{R_{pq}}, \tag{14}$$

in which $\sigma_{pq} = \sqrt{\sigma_p^2 + \sigma_q^2}$, is an effective width obtained from the Gaussian widths of oscillators p and q, that essentially determines the correlation length of this interaction potential. Since the dipole polarizability relates the response of a dipole moment to an applied electric field, the σ parameters physically correspond to the spatial spread of the local dipole moment distribution centered on a given oscillator. In fact, these Gaussian widths are directly related to the polarizability in classical electrodynamics [66] and can be derived from the dipole self-energy (*i.e.*, the zero-distance limit of the dipole-dipole interaction potential derived below in Eq. (15)) as $\sigma_p = (\sqrt{2/\pi}\,\alpha_p/3)^{1/3}$.

From Eq. (14), it is clear that this modified Coulomb potential satisfies both of the aforementioned conditions, so we now proceed to derive the dipole-dipole interaction tensor between two QHOs p and q from this modified Coulomb potential, which takes on the following form after straightforward algebra (*c.f.*, Eqs. (6) and (14)):

$$\begin{aligned}
\overline{\mathfrak{T}}_{pq}^{ab} &= \nabla_{\mathbf{R_p}} \otimes \nabla_{\mathbf{R_q}} \overline{v}_{pq} \\
&= -\frac{3R_aR_b - R_{pq}^2\delta_{ab}}{R_{pq}^5}\left(\text{erf}[R_{pq}/\sigma_{pq}] - \frac{2}{\sqrt{\pi}}\frac{R_{pq}}{\sigma_{pq}}\exp[-(R_{pq}/\sigma_{pq})^2]\right) \\
&+ \frac{4}{\sqrt{\pi}}\frac{R_aR_b}{\sigma_{pq}^3R_{pq}^2}\exp[-(R_{pq}/\sigma_{pq})^2].
\end{aligned} \tag{15}$$

We note that the above expression describes a potential that (*i*) attenuates the interaction between oscillators at short distances in comparison to the bare dipole-dipole interaction potential, converging to a finite value even in the zero-distance limit, and (*ii*) becomes equivalent to the bare dipole-dipole interaction potential for large interoscillator distances. Hence, the use of this range-separated dipole-dipole interaction potential for an arbitrary collection of QHOs not only allows us to avoid the near-field divergence that plagues the short-range, but also provides us with the simultaneous ability to correctly describe the long-range dispersion energy.

2.4 Electrodynamic Response Screening and Polarizability Anisotropy

Neglecting retardation effects due to the finite speed of light, the long-range dispersion energy between two atoms *in vacuo* originates from the electrodynamic interaction of "atomic" dipolar

fluctuations. However, when an atom is embedded in a condensed phase (or in a sufficiently large molecule), the corresponding dipolar fluctuations significantly differ from the free atom case, and in fact, this difference originates from *both* the local chemical environment surrounding the atom and the long-range electrodynamic interaction with the more distant fluctuating dipoles decaying *via* a $\sim 1/R^3$ power law. In other words, each atom located inside a molecule or material experiences a dynamic internal electric field created by both the local and non-local fluctuations associated with the surrounding atoms. Depending on the underlying topology of the chemical environment, this fluxional internal electric field can give rise to either polarization or depolarization effects, and is largely responsible for the anisotropy in the molecular polarizability tensor [67, 68]. Therefore, it is essential to include the environmental screening effects arising from both the short- and long-range in accurate first-principles calculations of the dispersion energy.

To address this issue, we again represent the N atoms in a given molecular system of interest as a collection of N QHOs, each of which is characterized by an isotropic frequency-dependent point dipole polarizability, the form of which is given in Eq. (4). Up to this point, we have yet to specify the parameters necessary to construct this polarizability for a given QHO, namely, an isotropic static dipole polarizability, α_p^0, and an effective excitation frequency, ω_p. From the discussion above, it is clear that we need to incorporate both short- and long-range environmental effects in our description of the QHO frequency-dependent polarizability in order to accurately capture the electrodynamic response screening and anisotropy effects. To account for the local chemical environment, we utilize the Tkatchenko-Scheffler (TS) prescription [25], in which $\alpha_p^0[\mathrm{n}(\mathbf{r})]$ and $\omega_p[\mathrm{n}(\mathbf{r})]$ are defined as functionals of the ground-state electron density, obtained from an initial self-consistent quantum mechanical calculation using either semi-local or hybrid DFT [69]—methods that can accurately treat electrostatics, induction, exchange-repulsion, and local hybridization effects, but lack the ability to describe long-range dispersion interactions [70]. Assuming that the system (whether it be an individual molecule, a collection of molecules, or even condensed matter), has a finite electronic gap and can therefore be divided into effective atomic fragments, the Hirshfeld, or stockholder [71], partitioning of the electron density is then utilized to account for the local chemical environment surrounding each atom. Since both parameters are referenced to highly accurate free-atom reference data, short-range quantum mechanical exchange-correlation effects are accounted for in these quantities by construction. In fact, the frequency-dependent polarizabilties defined in this manner yield C_6 coefficients that are accurate to 5.5% when compared to reference experimental values for an extensive database of atomic and (small) molecular dimers. Nevertheless, this parameterization of the frequency-dependent dipole polarizability clearly lacks the aforementioned long-range electrodynamic screening that extends beyond the range of the exponentially decaying atomic densities, and these effects must be accounted for self-consistently within this system of fluctuating oscillators.

To accurately capture the long-range electrodynamic response screening and anisotropy effects, we self-consistently solve the Dyson-like screening equation utilizing the range-separated dipole-dipole interaction tensor derived above in Eq. (15), thereby improving upon our initial description of the bare response function corresponding to this collection of QHOs. To proceed forward, we recall that this initial bare response function, χ_0, was constructed as a direct sum over the individual oscillator response functions given in Eq. (5), *i.e.*, $\chi_0 = \chi_0^p \oplus \chi_0^q \oplus \ldots$, which

now correspond to QHOs characterized by isotropic frequency-dependent dipole polarizabilities parameterized using the TS definitions for $\alpha_p^0[\mathrm{n}(\mathbf{r})]$ and $\omega_p[\mathrm{n}(\mathbf{r})]$ presented above. Therefore, the real-space matrix representation of χ_0 is diagonal and as a result, the corresponding self-consistent Dyson-like screening (SCS) equation is separable and can be recast as the following nonhomogeneous system of linear equations for a given frequency ω:

$$\overline{\alpha}_p(\mathrm{i}\omega) = \alpha_p(\mathrm{i}\omega) - \alpha_p(\mathrm{i}\omega)\sum_{q\neq p}^{N} \overline{\mathfrak{T}}_{pq}\overline{\alpha}_q(\mathrm{i}\omega) \qquad\qquad p = 1, 2, \ldots, N. \tag{16}$$

In Eq. (16), the complexity associated with integrating over spatial variables $\mathbf{r}$ and $\mathbf{r}'$ has been absorbed into $\overline{\mathfrak{T}}_{pq}$, the 3×3 block of the range-separated dipole-dipole interaction tensor in Eq. (15), which facilitates the use of overlapping spatially distributed frequency-dependent dipole polarizabilities by eliminating the issues associated with the near-field divergence. The set of $\overline{\alpha}_p(\mathrm{i}\omega)$ are the unknowns in the SCS equation and physically correspond to QHO dipole polarizabilities that account for both short-range (*via* the TS scheme) and long-range (*via* the solution of the SCS equation) electrodynamic response screening effects arising from the chemical environment. The solution of Eq. (16) with input polarizabilities computed at the TS level will be referred to as TS+SCS throughout the remainder of this work.

The SCS equation can be solved in matrix form *via* inversion of the $3N \times 3N$ Hermitian $\overline{A}$ matrix, which contains the inverse of the atomic frequency-dependent dipole polarizability tensors, $\alpha_p^{-1}(\mathrm{i}\omega)$, along the diagonal 3×3 atomic subblocks, and the range-separated dipole-dipole coupling tensor, $\overline{\mathfrak{T}}_{pq}$, in each of the corresponding 3×3 non-diagonal subblocks. Inversion of $\overline{A}$ yields the fully screened polarizability matrix, $\overline{B}$, from which one can obtain the fully screened *molecular* polarizability tensor by internally contracting over all atomic subblocks, $\overline{\alpha} = \sum_{pq}^{N} \overline{B}_{pq}$ and the fully screened set of *atomic* polarizability tensors by partial internal contraction $\overline{\alpha}_p = \sum_{q}^{N} \overline{B}_{pq}$. From these screened atomic polarizability tensors, $\overline{\alpha}_p^0$ and $\overline{\omega}_p$ can be obtained for each atom as described in Ref. [32] and will be used to compute the full many-body dispersion energy in the next section.

2.5 The Many-Body Dispersion Energy: The DFT+MBD Method

To compute the full many-body dispersion (MBD) energy, we represent the N atoms in a given molecular system of interest as a collection of QHOs, each of which is now characterized by a screened static dipole polarizability, $\overline{\alpha}_p^0$, and screened excitation frequency, $\overline{\omega}_p$, computed at the TS+SCS level of theory. We then directly solve the Schrödinger equation for this set of fluctuating and interacting QHOs within the dipole approximation, with the corresponding Hamiltonian [72, 73, 74, 75, 76]:

$$H = -\frac{1}{2}\sum_{p=1}^{N} \nabla_{\boldsymbol{\mu}_p}^2 + \frac{1}{2}\sum_{p=1}^{N} \overline{\omega}_p^2 \mu_p^2 + \sum_{p>q}^{N} \overline{\omega}_p \overline{\omega}_q \sqrt{\overline{\alpha}_p^0 \overline{\alpha}_q^0}\, \boldsymbol{\mu}_p \widetilde{\mathfrak{T}}_{pq} \boldsymbol{\mu}_q, \tag{17}$$

in which $\boldsymbol{\mu}_p = \sqrt{m_p}\boldsymbol{\xi}_p$ is defined in terms of $\boldsymbol{\xi}_p$, the displacement of a given QHO p from its equilibrium position, and $m_p = (\overline{\alpha}_p^0 \overline{\omega}_p^2)^{-1}$. In Eq. (17), the first two terms correspond to the single-particle kinetic and potential energy, respectively. The last term in the Hamiltonian describes the coupling between QHOs *via* the dipole-dipole interaction tensor ($\widetilde{\mathfrak{T}}_{pq} = \nabla_{\mathbf{R}_p} \otimes \nabla_{\mathbf{R}_q} W(R_{pq})$, where $W(R_{pq})$ will be defined below).

For a system of coupled QHOs, we have in fact proven the equivalence [77] between the full interaction energy obtained from the diagonalization of the Hamiltonian in Eq. (17) and the ACFD-RPA correlation energy expression in Eq. (3). Therefore, the full ACFD-RPA correlation energy can be efficiently computed by diagonalizing the $3N \times 3N$ Hamiltonian matrix. Hence, the MBD energy is computed as the difference between the zero-point energies of the coupled (collective) and uncoupled (single-particle) QHO frequencies, *i.e.*,

$$E_{\mathrm{MBD}} = \frac{1}{2}\sum_{p=1}^{3N}\sqrt{\lambda_p} - \frac{3}{2}\sum_{p=1}^{N}\overline{\omega}_p = E_{c,\mathrm{RPA}}, \tag{18}$$

in which λ_p are the Hamiltonian matrix eigenvalues.

Although the MBD energy is part of the long-range correlation energy, the full correlation energy in general also includes other contributions. In order to construct an electronic structure method that treats the full range of exchange and correlation effects, we need to couple the MBD energy in Eq. (18) to an approximate semilocal DFT functional. Instead of utilizing an *ad hoc* damping function, as typically employed in interatomic pairwise approaches, the coupling of MBD to an underlying functional (DFT+MBD) is achieved via the following range-separated Coulomb potential [78, 79], which suppresses the short-range interactions that are already captured at the DFT level,

$$W(R_{pq}) = \left(1 - \exp(-(R_{pq}/\overline{R}_{pq}^{\mathrm{vdW}})^{\beta})\right)/R_{pq}, \tag{19}$$

where β is a range-separation parameter that controls how quickly $W(R_{pq})$ reaches the long-range $1/R_{pq}$ asymptote, and $\overline{R}_{pq}^{\mathrm{vdW}} = \overline{R}_{p}^{\mathrm{vdW}} + \overline{R}_{q}^{\mathrm{vdW}}$ are the screened vdW radii as defined in Refs. [25, 32].

The value of the single range-separation parameter, β, is obtained from global optimization of the total DFT+MBD energy on the S22 test set, a widely employed benchmark database of noncovalent intermolecular interactions [80, 81]. For the PBE [82] and PBE0 [83, 84] functionals, the optimized values of the β parameter were found as 2.56 and 2.53, respectively.

Finally, we remark that our choice of using the screened $\overline{\alpha}_p^0$ and $\overline{\omega}_p$ parameters as input in Eq. (17) is not unique. Other choices are certainly possible from the viewpoint of the ACFD formula and we will investigate such alternatives in more detail in future work. In addition, the coupling of the long-range MBD energy to a semilocal or hybrid DFT functional distinguishes the DFT+MBD method from the widely used RPA@DFT approaches [43, 44, 45, 46, 47, 48, 49, 50, 51, 52, 53, 54, 55, 56, 57, 58] for computing the electron correlation energy. Furthermore, the MBD energy can be efficiently computed by diagonalizing the $3N \times 3N$ Hamiltonian matrix, enabling MBD calculations for thousands of atoms on a single processor.

3 Applications: The Role of Self-Consistent Electrodynamic Screening in the Molecular Polarizability

The simplest possible model for the polarizability of molecules and solids consists of a sum over effective hybridized polarizable atoms, as given by Eq. (4). This model can be very effective in reproducing accurately known isotropic molecular polarizabilities and isotropic C_6 coefficients.

For example, the TS method uses a localized atom-based model and yields an accuracy of $\approx 14\%$ for the isotropic polarizabilities of more than 200 molecules [85] and 5.5% for the C_6 coefficients in 1225 cases [25]. However, one has to recognize that the polarizability measures the response of a dipole moment to an applied electric field. Since both the dipole moment and the electric field are vector quantities, the dipole polarizability is evidently anisotropic and should be described by a second-rank tensor. Hence, the rather simplified additive model fails to correctly capture the anisotropy in the molecular polarizability [2]. Within the framework of electronic structure calculations, the static polarizability can be computed as the second derivative of the total energy with respect to an applied electric field. An alternative, but equivalent formulation for computing the polarizability is based on the fact that the single-particle orbitals in a molecule are electrodynamically coupled. The solution of the coupling equations leads to the many-electron frequency-dependent polarizability of the full system.

The TS+SCS method introduced above in Eq. (16) is based on such an electrodynamic interaction model. Upon obtaining effective isotropic parameters for atoms in a molecule or a solid from the ground-state electron density, the non-local polarizability tensor is determined from the solution of a system of dipole–dipole coupling equations. The dipole–dipole coupling between atoms naturally introduces anisotropy in the molecular polarizability, even if we start with purely isotropic atomic polarizabilities. We now illustrate the importance of electrodynamic screening for three different cases: small and medium-size molecules, a linear chain of H_2 molecules, and silicon clusters of increasing size.

3.1 Small and Medium-Size Molecules

Table 1 shows the three components of the molecular static polarizability, α_{xx}, α_{yy}, and α_{zz}, along with the isotropic static polarizability, $\alpha_{\rm iso}$, for a database of 18 molecules [68]. The TS atomic partitioning of the polarizability integrated in different directions yields a mean absolute error of 13.2% for the isotropic molecular polarizability, and a much larger error of 76.3% for the fractional anisotropy (FA), defined as

$$\mathrm{FA} = \sqrt{\frac{1}{2}\frac{(\alpha_{xx}-\alpha_{yy})^2+(\alpha_{xx}-\alpha_{zz})^2+(\alpha_{yy}-\alpha_{zz})^2}{\alpha_{xx}^2+\alpha_{yy}^2+\alpha_{zz}^2}}. \tag{20}$$

Upon including screening effects using the TS+SCS model [Eq. (16)], the isotropic polarizability is improved to 9.1%, and, more importantly, the accuracy of FA is improved by a factor of two to 33.5%. We suggest that a substantial part of the remaining error stems from the isotropic input into the SCS model. Using the full electron density anisotropy at the TS level requires a substantial extension of the TS+SCS model, which is work that is currently in progress. We note that for the calculation of the vdW energy, what matters is the integration of the polarizability over imaginary frequencies, $\alpha(\mathrm{i}\omega)$, hence the error in the static polarizability is ameliorated when computing the vdW energy.

For a pair of atoms or molecules A and B, the C_6^{AB} coefficient determines their long-range vdW interaction energy. One of the main achievements of the TS method consists of a parameter-free definition to determine the C_6^{AB} coefficients with an accuracy of 5.5% for a broad variety of small and medium-size molecules (1225 C_6^{AB} coefficients). The performance of the TS method

Table 1: The isotropic polarizability $\alpha_{\rm iso}$, along with its three components α_{xx}, α_{yy}, and α_{zz} (in bohr^3) for a database of molecules with reference data taken from Ref. [68]. The MARE for the components corresponds to the error in the fractional anisotropy (see text). The results are reported for the TS method (with anisotropy computed from the Hirshfeld partitioning, where the $\mathbf{r}^3$ operator is partitioned as $(xx+yy+zz)\mathbf{r}$), and the TS+SCS method.

	Experiment				TS				TS+SCS			
molecule	$\alpha_{\rm iso}$	α_{xx}	α_{yy}	α_{zz}	$\alpha_{\rm iso}$	α_{xx}	α_{yy}	α_{zz}	$\alpha_{\rm iso}$	α_{xx}	α_{yy}	α_{zz}
H_2	5.33	4.86	4.86	6.28	4.61	4.57	4.63	4.63	3.98	3.15	3.15	5.64
N_2	11.88	9.79	9.79	16.06	12.59	12.02	12.02	13.73	11.24	8.79	8.79	16.14
O_2	10.80	8.17	8.17	15.86	10.03	10.02	10.02	10.06	9.86	7.61	7.61	14.36
CO	13.16	11.00	11.00	17.55	14.62	13.80	13.80	16.27	13.21	10.76	10.76	18.13
ethane	30.23	26.86	26.86	37.05	33.72	33.18	33.18	34.79	31.86	28.78	28.79	38.02
propane	43.05	38.74	38.74	51.69	49.04	47.68	48.88	50.55	46.66	39.75	42.79	57.43
cyclopentane	61.75	56.69	61.88	66.67	74.56	72.49	75.56	75.63	68.49	57.54	73.95	73.98
cyclohexane	74.23	63.30	79.70	79.70	90.59	88.36	91.70	91.70	83.27	67.91	90.96	90.96
dimethylether	35.36	29.63	33.34	43.05	39.24	38.53	39.47	39.70	37.82	32.11	32.70	48.66
P-dioxane	58.04	47.24	63.43	63.43	70.50	69.68	70.17	71.64	65.76	53.12	67.20	76.97
methanol	22.40	17.88	21.80	27.60	24.44	23.99	24.61	24.72	23.11	19.96	21.44	27.92
ethanol	34.28	30.37	33.61	38.87	39.71	38.73	39.15	41.23	37.64	32.33	37.28	43.29
formaldehyde	16.53	12.35	18.63	18.63	19.06	17.09	19.54	20.55	18.09	11.42	18.86	24.00
acetone	43.12	29.83	49.74	49.74	49.07	45.80	50.22	51.18	48.05	35.41	49.90	58.83
acetonitrile	30.23	25.98	25.98	38.74	32.51	31.17	31.17	35.19	32.82	23.62	23.62	51.22
$(CH_3)_3CCN$	64.72	60.94	60.94	72.27	79.13	78.16	78.16	81.07	77.09	70.65	70.65	89.98
methane	17.68	17.68	17.68	17.68	18.90	18.90	18.90	18.90	17.39	17.39	17.39	17.39
benzene	69.70	45.10	82.00	82.00	75.29	71.82	77.02	77.03	71.95	33.02	91.41	91.42
MARE	-	-			13.2%	76.3%			9.1%	33.5%		

is shown in Figure 1, where a remarkable correlation can be seen with reliable C_6^{AB} values computed from the experimental dipole-oscillator strength distributions (see Ref. [25] for a detailed analysis). The reason behind such a good performance is that SCS effects beyond semilocal hybridization largely average out when computing C_6 coefficients for small molecules. In fact, the TS+SCS method yields an accuracy of 6.3% for the aforementioned 1225 C_6 coefficients and its performance is also shown in Figure 1. We attribute the slight increase of the error with respect to TS as stemming from the approximation of the dipole moment distribution by a single isotropic QHO. The largest errors of TS+SCS are found for linear alkane chains, where the anisotropy along the chain is overestimated. Full tensor formulation of the input TS polarizabilities is under way and preliminary results indicate that the molecular anisotropy is improved.

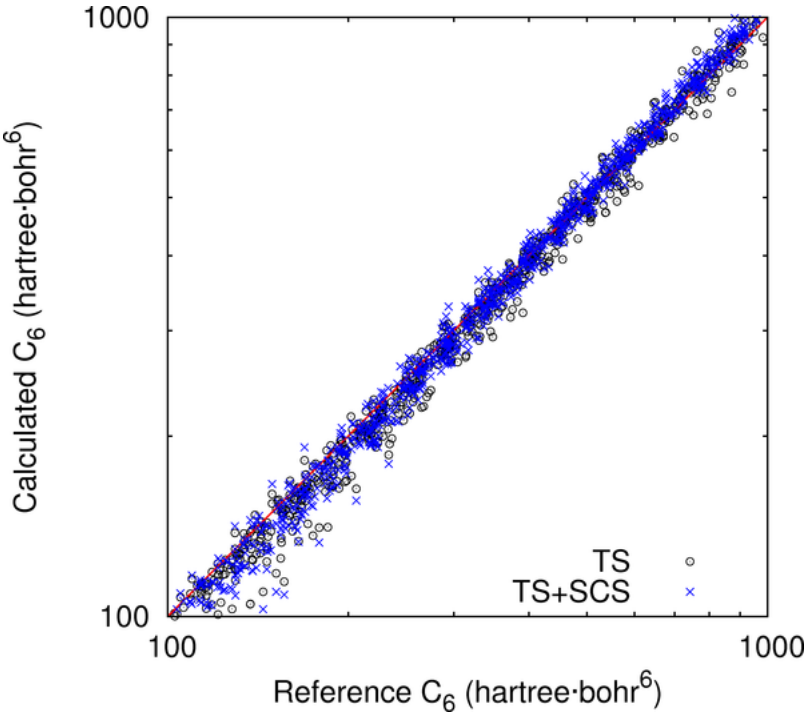

Figure 1: Isotropic C_6 coefficients for a database of 50 atoms and molecules (1225 data points) computed with TS and TS+SCS methods, compared with reliable DOSD values (see text).

3.2 Linear Chain of H_2 Molecules

We further illustrate the importance of SCS effects with the example of the linear $(H_2)_3$ chain, consisting of three H_2 dimers with alternating bond lengths (2 bohr inside the dimer and 3 bohr between the dimers). An accurate calculation of the polarizability of such hydrogen dimer chains is considered to be a significant challenge for electronic structure theory [86]. We have calculated the reference frequency-dependent polarizability for $(H_2)_3$ using the linear-response coupled-cluster method (LR-CCSD) as implemented in the NWChem code [87, 88]. The LR-CCSD method is a state-of-the-art approach for computing static and frequency-dependent molecular polarizabilities, and it yields results that agree to ≈3% when compared to reliable experimental values. The results for the isotropic and anisotropic C_6 coefficients for this chain at the TS, TS+SCS, and LR-CCSD levels of theory are shown in Table 2. The TS method yields a vanishingly small anisotropy in the C_6 coefficient since it only accounts for the local environment. On the contrary, TS+SCS correctly captures the dipole alignment (polarization) along the $(H_2)_3$ chain, leading to a significant anisotropy that is in fair agreement with the reference LR-CCSD values. Also, the isotropic C_6 coefficient is noticeably improved when using the TS+SCS approach in comparison to TS.

3.3 Silicon Clusters

We have shown that the TS+SCS method can rather effectively describe the anisotropy and polarization effects in molecules. We now illustrate that the TS+SCS approach can also accurately treat depolarization in clusters and solids with the example of hydrogen-saturated silicon clus-

Table 2: Anisotropic ($C_{6,\perp}$, $C_{6,||}$) and isotropic ($C_{6,\mathrm{iso}}$) C_6 coefficients for the linear $(H_2)_3$ chain using the TS and TS+SCS methods. Reference linear-response coupled-cluster (LR-CCSD) results are also shown. All values in hartree·bohr^6.

	$C_{6,\perp}$	$C_{6,||}$	$C_{6,\mathrm{iso}}$
TS	166	161	165
TS+SCS	89	692	223
LR-CCSD	115	638	238

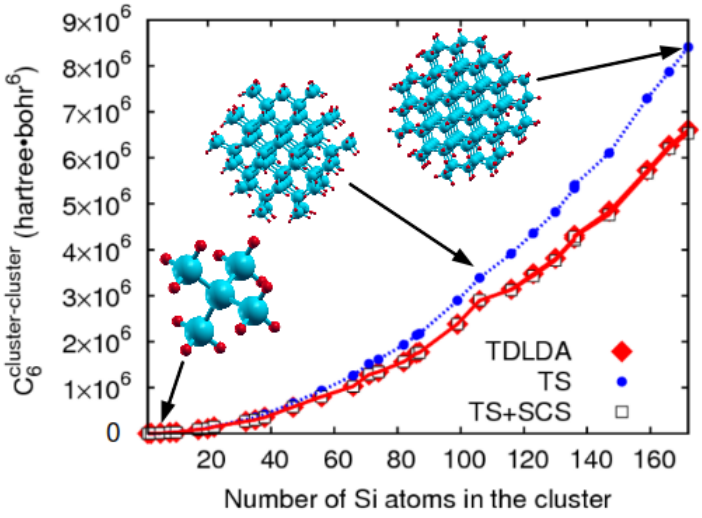

Figure 2: Cluster–cluster isotropic C_6 coefficients for hydrogen-terminated silicon clusters of increasing size. The TDLDA results are from Ref. [89].

ters of increasing size. The cluster–cluster C_6 coefficients are shown in Figure 2. The reference values correspond to the TDLDA calculations of S. Botti *et al.* [89]. We measured the accuracy of TDLDA using the experimentally derived C_6 coefficient for the SiH_4 molecule [90] and the $C_6^{\mathrm{Si-Si}}$ coefficient in the silicon bulk determined from the Clausius-Mossotti equation with the experimental dielectric function. For the SiH_4 molecule, TDLDA yields a 13% overestimation and this error is further reduced to 3% for the silicon bulk. Therefore, we deem the TDLDA C_6 coefficients as good references for the larger silicon clusters. For smaller clusters, the TS values are accurate and are in good agreement with experiment and TDLDA as expected. However, the error in the TS method increases progressively with the cluster size. For the largest $Si_{172}H_{120}$ cluster, the TS approach yields an overestimation of 27%. TS+SCS leads to an overall depolarization for the larger clusters, decreasing the error significantly in comparison to TDLDA. The depolarization effect is even larger for the Si bulk. The TS scheme yields an overestimation of 68% in the $C_6^{\mathrm{Si-Si}}$ coefficient in comparison to the value derived from the experimental dielectric function, while the TS+SCS approach reduces the overestimation to just 8%.

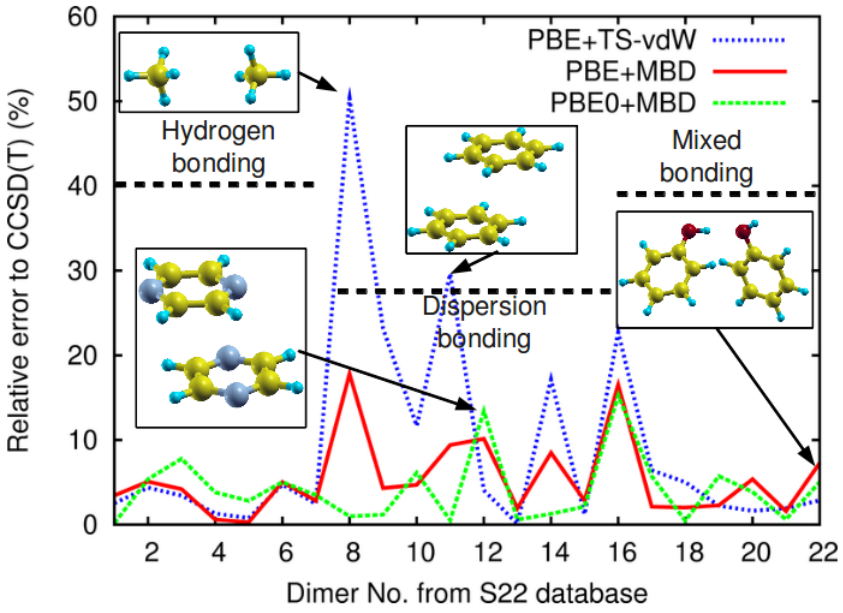

Figure 3: The performance of the PBE+TS-vdW method of Tkatchenko and Scheffler [25], PBE+MBD, and PBE0+MBD methods on the S22 database of intermolecular interactions. The error is reported to the basis-set converged CCSD(T) results of Takatani *et al.* [81].

4 Applications: Performance of the DFT+MBD Method

Having established the accuracy of the TS+SCS method for computing the vdW coefficients for a wide variety of systems from molecules to solids, we now assess the performance of the DFT+MBD method based on the TS+SCS input (see Section 2.5) for a broad variety of molecular systems. The cases studied herein include the binding energies of molecular dimers, conformational energetics of extended and globular alanine tetrapeptide, binding in the supramolecular host–guest buckyball catcher complex, as well as cohesion in molecular crystals composed of oligoacenes. The all-electron numeric atom-centered orbital code FHI-aims [91] was utilized for the DFT calculations discussed in this work.

4.1 Intermolecular Interactions: The S22 and S66 Databases

In order to assess the performance of the DFT+MBD method, we first study the S22 database of intermolecular interactions [80], a widely used benchmark database for which reliable binding energies have been calculated using high-level quantum chemical methods [80, 81]. In particular, we use the recent basis-set extrapolated CCSD(T) binding energies calculated by Takatani *et al.* [81]. These binding energies are presumed to have an accuracy of $\approx$ 0.1 kcal/mol (1% relative error), and this level of accuracy is required for an unbiased assessment of approximate approaches for treating dispersion interactions.

Figure 3 shows the performance of the DFT+MBD method on the S22 database when used with the standard semilocal PBE [82] functional and the hybrid PBE0 [83, 84] functional which includes 25% Hartree-Fock exchange. The inclusion of the many-body vdW energy leads to a remarkable improvement in accuracy compared to the PBE+TS-vdW method [25]. The largest

improvement when using the MBD energy over the pairwise TS-vdW energy is observed for the methane dimer and the parallel-displaced benzene dimer. We note that the methane dimer is bound by only 0.53 kcal/mol at the CCSD(T) level of theory, and the MBD energy reduces the binding by 0.19 kcal/mol with respect to TS-vdW, explaining the large reduction in error seen in Figure 3. This reduction does not come mainly from the many-body dispersion energy, rather it is due to a more physical definition of the short-range interactions in the MBD method arising from a range-separated Coulomb potential [32]. Taking the second-order expansion of the MBD energy, which yields a strictly pairwise energy, leads to a change of only 0.05 kcal/mol [77] compared to the full MBD energy. This simple test illustrates that the main difference between PBE+TS-vdW and PBE+MBD for the methane dimer stems from the different way of treating the short-range dispersion interactions. In addition, the inclusion of Hartree-Fock exchange in the PBE0 functional allows for a better description of permanent electrostatic moments and static polarizabilities for molecules, and leads to improved binding energies when compared to the semilocal PBE functional. We note that there are two systems in the S22 database for which the relative PBE0+MBD error exceeds 10% when compared to the CCSD(T) binding energies: pyrazine dimer (system 12) and ethene–ethyne (system 16). We attribute this finding to the remaining inaccuracy in the anisotropy for the molecular polarizabilities computed with the TS+SCS method. This issue will be analyzed in more detail for the case of the buckyball catcher complex below.

Table 3: Performance of different methods on the S22 database of intermolecular interactions, measured in terms of the mean absolute relative error (MARE, in %). The errors are measured with respect to the basis-set extrapolated CCSD(T) calculations of Takatani *et al.* [81]. The error is reported for hydrogen-bonded (H-B), dispersion-bonded (D-B), and mixed (M-B) systems. The number of empirical parameters used in every approach is shown in the "N. param." column. Results are shown for MP2, EX+cRPA, EX+cRPA+SE [57], vdW-DF1 and vdW-DF2 [23], rPW86+cPBE+VV10 [24, 92], PBE0-D3 [28], PBE0+TS-vdW [25, 26], and PBE0+MBD [32].

Method	H-B	D-B	M-B	Overall	N. param.
MP2	1.8	37.4	14.8	18.9	0
EX+cRPA	11.2	21.6	14.8	16.1	0
vdW-DF1	15.2	13.0	10.8	13.0	0
PBE0-D3(Grimme)	8.4	15.5	12.7	12.3	> 3
EX+cRPA+SE	5.9	11.6	5.4	7.8	0
vdW-DF2	5.3	6.8	10.8	7.6	1
PBE0+TS-vdW	3.4	12.0	6.0	7.3	2
rPW86+cPBE+VV10	6.1	2.6	4.8	4.4	2
PBE0+MBD	4.1	3.4	5.1	4.2	1

To put the performance of the DFT+MBD method in the context of other currently available approaches, we show the mean absolute relative errors (MARE) on the S22 database for a variety of state-of-the-art methods in Table 3 and in Figure 4. The number of empirical parameters employed for the dispersion energy in every method is also enumerated in Table 3. Only the PBE0+MBD method [32] and the rPW86+cPBE+VV10 approach [24, 92] yield consistent per-

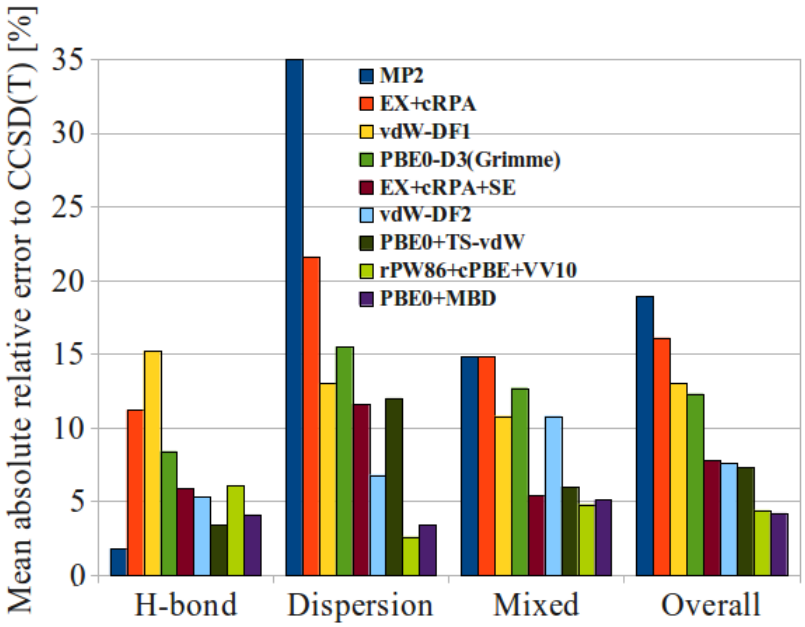

Figure 4: Performance of different methods on the S22 database of intermolecular interactions, measured in terms of the mean absolute relative error (MARE, in %). The errors are measured with respect to the basis-set extrapolated CCSD(T) calculations of Takatani *et al.* [81]. Results are shown for MP2, EX+cRPA, EX+cRPA+SE [57], vdW-DF1 and vdW-DF2 [23], rPW86+cPBE+VV10 [24, 92], PBE0-D3 [28], PBE0+TS-vdW [25, 26], and PBE0+MBD [32].

formance with errors below 6% with respect to the CCSD(T) reference data for all interaction types. We note that the rPW86+cPBE+VV10 method uses two empirical parameters in the expression for the dispersion energy, while the PBE0+MBD method uses only a single range-separation parameter for the coupling of the long-range dispersion energy to the underlying DFT functional.

Recently, Hobza's group has significantly revised and extended the S22 database to include a broader variety of molecules and intermolecular interactions. The result of this effort is the so-called S66 database, composed of 66 molecular dimers [93]. The reference binding energies for the S66 database have been computed at the CCSD(T) level of theory employing medium-size basis sets, with an expected accuracy of ≈2-3% from the basis set limit. In order to cover non-equilibrium geometries, CCSD(T) binding energies have also been computed for 8 different intermolecular separations, ranging from a factor of 0.9 to 2.0 of the equilibrium distances. Therefore, the so-called S66x8 database contains binding energies for a total of 528 complexes computed at the CCSD(T) level of theory. The performance of the PBE0+MBD approach on the S66 database is comparable to the S22 results presented above. For equilibrium geometries in the S66 database, the mean absolute error (MAE) and MARE of the PBE0+MBD method are 0.38 kcal/mol and 6.1%, respectively. When all 528 equilibrium and non-equilibrium complexes are taken into account, the calculated MAE and MARE are 0.37 kcal/mol and 8.5%, respectively. The increase in the MARE stems from the S66(0.9x) and S66(0.95x) complexes with shorter-than-equilibrium interaction distances. This is a well-known weakness of all dispersion-inclusive DFT methods, with errors increasing when considering shorter distances, since the dispersion

energy contribution for such distances becomes very small.

We conclude that the MBD energy beyond the standard pairwise approximation is important even when studying the binding between rather small molecules. Empirical pairwise methods for the dispersion energy mimic some of the higher-order effects by adjusting sufficiently flexible damping functions, but this strategy is prone to fail for different molecular conformations and for more complex molecular geometries. We illustrate one such case in the next subsection.

4.2 Intramolecular Interactions: Conformational Energies of Alanine Tetrapeptide

The study of biomolecules in the gas phase corresponds to ideal "clean room" conditions, and recent progress in experimental gas-phase spectroscopy has yielded increasingly refined vibrational spectra for peptide secondary structures [94, 95, 96]. Joint experimental and *ab initio* theoretical studies can now successfully determine the geometries of small gas-phase peptides [97, 98, 99]. Polyalanine is a particularly good model system due to its high propensity to form helical structures [100], and its widespread use as a benchmark system for peptide stability in experiments and theory.

Here we assess the accuracy of the PBE0+MBD method for 27 conformations of alanine tetrapeptide (Ace-Ala_3-NMe, for brevity called Ala_4 here), for which benchmark CCSD(T) conformational energies were computed in Ref. [101], based on converged MP2/CBS values from Refs. [102, 103]. The Ala_4 conformations range from a β-sheet-like fully extended structure to a globular ("folded") conformer. The wide variety of interactions present in peptides ranging from hydrogen bonds to dispersion and electrostatics makes an accurate prediction of the conformational hierarchy of these systems quite a daunting task for affordable electronic structure calculations. We illustrate the performance of PBE0+TS-vdW and PBE0+MBD for Ala_4 conformers in Figure 5. The PBE0+MBD method predicts a MAE of 0.29 kcal/mol with respect to the CCSD(T) reference, which is a significant reduction from 0.52 kcal/mol for PBE0+TS-vdW. We find that the main effect of the MBD energy over the pairwise TS-vdW approximation is to destabilize the extended conformations of Ala_4, bringing their energies in much better agreement with the reference CCSD(T) values.

4.3 Supramolecular Systems: The Buckyball Catcher

Supramolecular host–guest systems play an important role for a wide range of applications in chemistry and biology. The prediction of the stability of host–guest complexes represents a great challenge for first-principles calculations due to the interplay of a wide variety of covalent and non-covalent interactions in these systems. Here we assess the performance of the DFT+MBD method on the binding of the so-called "buckyball catcher" complex, $C_{60}@C_{60}H_{28}$, shown in Figure 6. Since its synthesis [105], the buckyball catcher has become one of the most widely used benchmark systems for supramolecular chemistry. Recently a reliable binding energy of 26 ± 2 kcal/mol has been determined for the $C_{60}@C_{60}H_{28}$ complex from large-scale diffusion Monte Carlo (DMC) calculations [63]. This value is in excellent agreement with an extrapolated binding energy determined from the experimentally measured binding affinity [29].

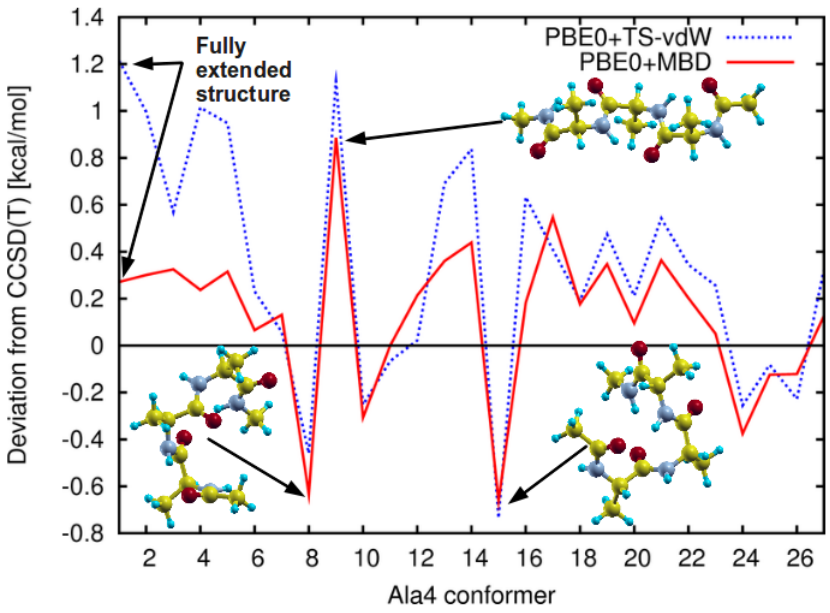

Figure 5: Performance of PBE0+TS-vdW and PBE0+MBD for the conformational energies of Ala_4. The reference CCSD(T) energies are taken from Ref. [101].

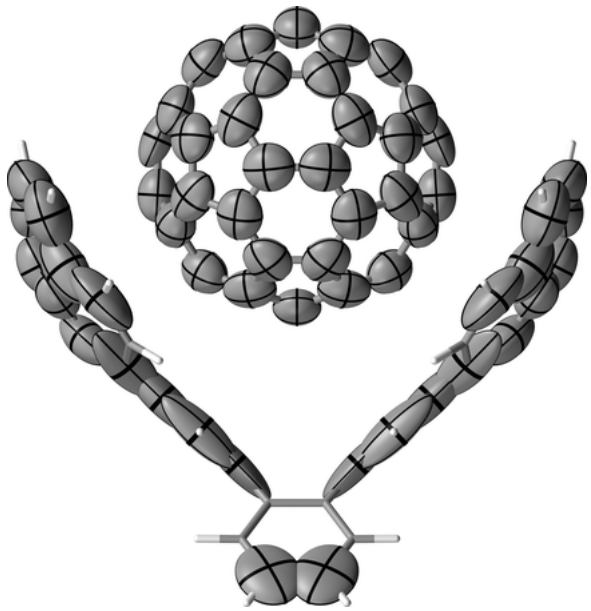

Figure 6: Illustration of the geometry and the anisotropy in the atomic TS+SCS polarizabilities of the $C_{60}@C_{60}H_{28}$ complex. The polarizability tensors are visualized as ellipsoids [104].

All pairwise-corrected dispersion-inclusive DFT calculations significantly overestimate the stability of the buckyball catcher complex, anywhere from 9 to 17 kcal/mol [63]. The PBE+MBD method yields a binding energy of 36 kcal/mol, improving the binding by 7 kcal/mol compared to the PBE+TS-vdW method. The inclusion of exact exchange using the PBE0+MBD method leads to a negligible change in the binding energy. Therefore, the PBE0+MBD method overestimates the binding by at least 8 kcal/mol compared to the DMC and extrapolated experimental reference binding energies.

In order to understand the most likely origin of why the binding energy of $C_{60}@C_{60}H_{28}$ complex is overestimated by PBE0+MBD, we show the projected polarizability tensors of the full complex resulting from the TS+SCS calculation in Figure 6. One can clearly see that the polarizability distribution is highly anisotropic, with an increasing anisotropy close to the linker moiety that connects the two corannulene molecules of the catcher complex. While the approximation of isotropic C_6 coefficients used in DFT+MBD becomes sufficient as the distance between the atoms is increased, at shorter interatomic distances the anisotropy plays a non-negligible role [62]. At present, there is no efficient method that can accurately account for the fully anisotropic dispersion energy at close interatomic distances. This statement applies to the widely employed interatomic dispersion energy methods, as well as the non-local density functionals (e.g., different variants of the vdW-DF method [11]). Work is currently in progress to seamlessly include anisotropy in dispersion energy expressions [77, 62]. The anisotropy in the atomic polarizabilities will change the vdW energy contribution in different directions. In the case of the $C_{60}@C_{60}H_{28}$ complex, the polarizability of the $C_{60}H_{28}$ molecule is highly anisotropic as shown in Figure 6. In the isotropic approximation, the dispersion energy between the C_{60} molecule and the corannulene moieties is therefore overestimated, because the polarization is artificially extended towards the C_{60} molecule. The fully anisotropic treatment of the dispersion energy is therefore likely to bring the binding energy closer to the DMC reference value.

4.4 Molecular Crystals

The understanding and prediction of the structure and stability of molecular crystals is of paramount importance for a variety of applications, including pharmaceuticals, non-linear optics, and hydrogen storage [106, 107]. The crystal structure prediction blind tests conducted by the Cambridge Crystallographic Data Centre have shown steady progress toward theoretical structure prediction for molecular crystals [108]. However, the insufficiency of DFT with pairwise dispersion corrections for the reliable predictions of molecular crystals is well documented, see e.g., Refs. [109, 110, 111, 27].

To illustrate the role of MBD interactions in the stability of molecular crystals, we have studied a series of oligoacene crystals from naphthalene to pentacene. We have recently shown that reliable structures of oligoacene crystals (2% accuracy compared to low-temperature X-ray data) can be obtained with PBE+TS-vdW calculations, while MBD interactions play only a minor role in determining the geometry of these molecular crystals [112]. However, the MBD energy plays a more significant role for the lattice energies of oligoacene crystals. Table 4 shows lattice energies at 0 K for naphthalene (2 benzene rings), anthracene (3 rings), tetracene (4 rings), and pentacene (5 rings) calculated using the PBE+TS-vdW and PBE+MBD methods, as well as a range of

measured sublimation enthalpies extrapolated to 0 K. We have only taken those experimental values that are recommended as reliable after critical revision by the authors of Ref. [113], thus avoiding anomalously small or large sublimation enthalpies. Both naphthalene and anthracene crystals have been rigorously studied, and their sublimation enthalpies are well known with a spread of 0.05 and 0.12 eV per molecule, respectively. There are fewer measurements available for tetracene and pentacene, and for the latter the three available experimental values deviate by 0.55 eV per molecule.

For naphthalene, anthracene, and tetracene, the PBE+MBD method decreases and improves the binding by about 0.1 eV (2.3 kcal/mol) per molecule when compared to PBE+TS-vdW. This is a notable improvement, especially if viewed in the context of intermolecular interactions for the S22 and S66 databases. We remind the reader that the errors of PBE+TS-vdW and PBE+MBD for molecular dimers in the S22/S66 databases are well below 0.5 kcal/mol. The much larger difference between the pairwise PBE+TS-vdW approach and the many-body PBE+MBD method for molecular crystals can be explained by the presence of significant electrodynamic screening effects in extended systems, that are virtually absent in small molecules. We refer the reader to Ref. [112] for a detailed analysis of the importance of electrodynamic screening in molecular crystals.

The remaining slight overestimation of lattice energies in Table 4 by PBE+MBD compared to the experimental range can be explained by the fact that the sublimation enthalpy is measured at finite temperatures, where the crystal unit cell undergoes thermal expansion. When using the experimental unit cell at 295 K for naphthalene, the PBE+MBD method yields a lattice energy that is increased by 50 meV per molecule, which places it essentially within the experimental range reported in Table 4. Finally, we studied the influence of exact exchange for oligoacene crystals, finding that the PBE0+MBD method leads to an almost negligible difference when compared to PBE+MBD; the lattice energy is decreased by only 10 meV/molecule when the PBE0+MBD functional is employed instead of PBE+MBD.

Table 4: Lattice energies of oligoacene crystals including zero-point energy (PBE+TS-vdW and PBE+MBD calculations were carried out using optimized PBE+TS-vdW geometries). The range of experimental ("Exp.") "lattice energies" from Ref. [113] and extrapolated to 0 K. All values are in units of eV per molecule.

	PBE+TS-vdW	PBE+MBD	Exp.
naphthalene	-0.950	-0.862	-0.803 to -0.752
anthracene	-1.324	-1.206	-1.148 to -1.024
tetracene	-1.666	-1.587	-1.525 to -1.299
pentacene	-2.035	-2.018	-2.082 to -1.533

Our current work on a broad dataset of molecular crystals and their polymorphs [114, 115] shows that beyond-pairwise many-body vdW interactions can be even more significant than found here for the oligoacene crystals.

5 Remaining Challenges

In this highlight we have described a recently developed method for the many-body vdW dispersion energy based on a system of quantum harmonic oscillators (QHO). The resulting DFT+MBD approach is parameter-free for the determination of the frequency-dependent polarizability, and uses a single range-separation parameter for the coupling between the long-range many-body vdW energy and a given DFT functional. We view the DFT+MBD model as a crucial first step in the development of a reliable (accurate and efficient) method for describing many-body vdW interactions in complex materials.

Currently, the DFT+MBD method essentially amounts to solving the ACFD-RPA correlation energy equation for a system of localized screened QHOs in the dipole (long-range) approximation. There are several important extensions that can be accomplished within the ACFD framework that would allow us to go beyond the DFT+MBD method:

1. **Improving the dipolar response.** The TS+SCS method defined in Eq. (16) yields the full non-local interacting response matrix as a function of atomic positions $\mathbf{r}$ and $\mathbf{r}'$. Currently, this information is not fully utilized in the DFT+MBD approach, since we use contracted isotropic TS+SCS atomic polarizabilities as input for the ACFD-RPA formula. In principle, the full response matrix can be used in the ACFD-RPA expression, however this requires a matching definition for the range-separated Coulomb potential. The interacting TS+SCS response matrix transforms the original atom-based representation to an eigenvector representation for the coupled modes of the system. The Coulomb interaction between the coupled modes needs to be extended from our current definition of range-separation that is based on atomic vdW radii.

2. **Going beyond the dipole approximation.** The QHO model possesses a response to infinite order in the multipole expansion. The current MBD method restricts the response to the dipole approximation, effectively allowing excitations only to the first excited state for every QHO due to the dipole selection rule. In principle, the full response function given by Eq. (2) can be computed for a system of QHOs up to an arbitrary energy cutoff for the excited states. This would allow us to treat multipole responses higher than dipole (quadrupole, octupole, etc.). The ACFD-RPA expression can still be utilized in this case, allowing us to compute dispersion interactions at shorter interatomic distances. It remains to be assessed whether or not this model will be useful, as a single QHO per atom might not be able to properly describe vdW interactions at shorter interatomic distances. However, in principle, our method can also be extended to represent every atom by several QHOs.

3. **Coupling between the long-range vdW energy and the DFT energy.** The DFT+MBD method couples the long-range vdW energy to the DFT energy by using a single range-separation parameter in the Coulomb potential. In order to improve this empirical component of the DFT+MBD method, the DFT functional has to be derived in the presence of the long-range vdW energy. To date, we have not used the fact that different functionals yield different results for the electron density tails; this information can be useful for developing a functional in which the long-range vdW energy is seamlessly integrated with the semilocal exchange-correlation functional.

4. **Simultaneous description of localized and metallic states.** Successful non-empirical DFT functionals are based on the local-density approximation (LDA) and converge to the LDA in the homogeneous electron gas (HEG) limit. LDA is an exact functional for the HEG, hence it includes vdW interactions inside the HEG. Therefore, a seamless vdW functional should yield a vanishing correction for the HEG. This can easily be accomplished by letting the polarizability vanish for slowly-varying regions of the electron density, as done in the vdW-DF [22] and VV10 [92] approaches. However, real materials (transition metals, nanostructures, etc.) are more complex than the rather simplified HEG model. In such systems, vdW interactions between ions are significant and are *screened* by the itinerant metallic electrons [116]. State-of-the-art vdW functionals do not correctly describe this complex situation. However, the DFT+MBD method can be extended to systems with localized and metallic states by introducing both localized and delocalized oscillators for every atom. The challenge consists of defining the oscillator parameters directly from the electron density and its gradient.

5. **Interatomic forces, geometry optimization, and molecular dynamics.** Currently, the DFT+MBD method only yields the total energy for a specified geometry. In principle, geometry optimizations are possible by using the finite difference approximation for the interatomic forces. This is, however, computationally expensive especially in the case of molecular dynamics. Work is in progress to derive an analytic expression for the interatomic forces corresponding to the MBD energy. Such development would allow for the routine application of the DFT+MBD method in large-scale molecular dynamics simulations.

6 Conclusions

There is mounting evidence that many-body vdW interactions, beyond the standard pairwise approximation, play a crucial role in the structure, stability, and function of a wide variety of systems of importance in biology, chemistry, and physics. In this highlight, we have illustrated the importance of including many-body vdW interactions when describing small molecular dimers, conformational energies of peptides, binding in supramolecular systems, and cohesion in molecular crystals. We presented a derivation of both the pairwise and many-body interatomic vdW dispersion energy from the exact quantum-mechanical ACFD-RPA correlation energy expression. The ACFD formula provides us with a powerful framework for the understanding and future development of accurate and efficient electronic structure approaches.

The DFT+MBD method [32, 33] represents a first step towards the development of reliable methods for describing many-body vdW interactions in complex materials. In this work, we derived the MBD energy expression from the exact ACFD formula, discussed the approximations involved, and identified the remaining challenges that need to be addressed in future work. Over the next few years, we anticipate extensive development of new dispersion energy methods that will address the truly collective many-body nature of these ubiquitous quantum-mechanical forces.

7 Acknowledgements

The authors acknowledge the European Research Council (ERC Starting Grant VDW-CMAT) for support, and thank M. Scheffler, R. Car, X. Ren, J. F. Dobson, O. A. von Lilienfeld, A. Ambrosetti, A. M. Reilly, and N. Marom for enlightening discussions. R.A.D. was supported by the DOE under Grant No. DE-SC0005180 and by the NSF under Grant No. CHE-0956500.

References

[1] V. A. Parsegian, *Van der Waals forces: A Handbook for Biologists, Chemists, Engineers and Physicists* (Cambridge University Press, 2005).

[2] A. J. Stone, *The Theory of Intermolecular Forces* (Oxford University Press, 1996).

[3] I. G. Kaplan, *Intermolecular Interactions: Physical Picture, Computational Methods and Model Potentials* (John Wiley and Sons, 2006).

[4] R. French *et al.*, Rev. Mod. Phys. **82**, 1887 (2010).

[5] B. Jeziorski, R. Moszynski and K. Szalewicz, Chem. Rev. **94**, 1887 (1994).

[6] P. Loskill, H. Hähl, T. Faidt, S. Grandthyll, F. Müller and K. Jacobs, Adv. Coll. Interf. Sci. **107**, 179182 (2012).

[7] P. Loskill, J. Puthoff, M. Wilkinson, K. Mecke, K. Jacobs and K. Autumn, J. R. Soc. Interface (2013), doi:10.1098/rsif.2012.0587.

[8] K. E. Riley, M. Pitonak, P. Jurecka and P. Hobza, Chem. Rev. **110**, 5023 (2010).

[9] F. O. Kannemann and A. D. Becke, J. Chem. Theory Comput. **6**, 1081 (2010).

[10] S. Grimme, Comput. Mol. Sci. **1**, 211 (2011).

[11] V. R. Cooper, L. Kong and D. C. Langreth, Physics Procedia **3**, 1417 (2010).

[12] S. Steinmann and C. Corminboeuf, J. Chem. Theory Comput. **7**, 3567 (2011).

[13] A. Tkatchenko, L. Romaner, O. T. Hofmann, E. Zojer, C. Ambrosch-Draxl and M. Scheffler, MRS Bull. **35**, 435 (2010).

[14] A. J. Misquitta, R. Podeszwa, B. Jeziorski and K. Szalewicz, J. Chem. Phys. **123**, 214103 (2005).

[15] O. A. von Lilienfeld, I. Tavernelli, U. Rothlisberger and D. Sebastiani, Phys. Rev. Lett. **93**, 153004 (2004).

[16] E. R. Johnson and A. D. Becke, J. Chem. Phys. **123**, 024101 (2005).

[17] P. L. Silvestrelli, Phys. Rev. Lett. **100**, 053002 (2008).

[18] G. Mercurio, E. R. McNellis, I. Martin, S. Hagen, F. Leyssner, S. Soubatch, J. Meyer, M. Wolf, P. Tegeder, F. S. Tautz and K. Reuter, Phys. Rev. Lett. **104**, 036102 (2010).

[19] N. Atodiresei, V. Caciuc, P. Lazic and S. Blügel, Phys. Rev. Lett. **102**, 136809 (2009).

[20] K. Tonigold and A. Gross, J. Chem. Phys. **132**, 224701 (2010).

[21] D. Stradi, S. Barja, C. Diaz, M. Garnica, B. Borca, J. J. Hinarejos, D. Sanchez-Portal, M. Alcami, A. Arnau, A. L. Vazquez de Parga, R. Miranda and F. Martin, Phys. Rev. Lett. **106**, 186102 (2011).

[22] M. Dion, H. Rydberg, E. Schroder, D. C. Langreth and B. I. Lundqvist, Phys. Rev. Lett. **92**, 246401 (2004).

[23] K. Lee, E. D. Murray, L. Kong, B. I. Lundqvist and D. C. Langreth, Phys. Rev. B **92**, 081101 (2010).

[24] O. A. Vydrov and T. Van Voorhis, J. Chem. Theory Comput. **8**, 1929 (2012).

[25] A. Tkatchenko and M. Scheffler, Phys. Rev. Lett. **102**, 073005 (2009).

[26] N. Marom, A. Tkatchenko, M. Rossi, V. V. Gobre, O. Hod, M. Scheffler and L. Kronik, J. Chem. Theory Comput. **7**, 3944 (2011).

[27] O. A. von Lilienfeld and A. Tkatchenko, J. Chem. Phys. **132**, 234109 (2010).

[28] S. Grimme, J. Antony, S. Ehrlich and H. Krieg, J. Chem. Phys. **132**, 154104 (2010).

[29] S. Grimme, Chem. Eur. J **18**, 9955 (2012).

[30] G.-X. Zhang, A. Tkatchenko, J. Paier, H. Appel and M. Scheffler, Phys. Rev. Lett. **107**, 245501 (2011).

[31] V. G. Ruiz, W. Liu, E. Zojer, M. Scheffler and A. Tkatchenko, Phys. Rev. Lett. **108**, 146103 (2012).

[32] A. Tkatchenko, R. A. DiStasio, Jr., R. Car and M. Scheffler, Phys. Rev. Lett. **108**, 236402 (2012).

[33] R. A. DiStasio Jr., O. A. von Lilienfeld and A. Tkatchenko, Proc. Natl. Acad. Sci. USA **109**, 14791 (2012).

[34] J. F. Dobson and T. Gould, Calculation of Dispersion Energies, `http://www.psi-k.org/newsletters/News_107/Highlight_107.pdf`, 2011.

[35] J. Klimes and A. Michaelides, J. Chem. Phys. **137**, 120901 (2012).

[36] Towards First-Principles Description of van der Waals Interactions in Complex Materials, `http://www.cecam.org/workshop-791.html`, 2012.

[37] O. Gunnarsson and B. I. Lundqvist, Phys. Rev. B **13**, 4274 (1976).

[38] D. C. Langreth and J. P. Perdew, Phys. Rev. B **15**, 2884 (1977).

[39] S. L. Adler, Phys. Rev. **126**, 413 (1962).

[40] N. Wiser, Phys. Rev. **129**, 62 (1963).

[41] D. Bohm and D. Pines, Phys. Rev. **92**, 609 (1953).

[42] M. Gell-Mann and K. A. Brueckner, Phys. Rev. **106**, 364 (1957).

[43] M. Fuchs and X. Gonze, Phys. Rev. B **65**, 235109 (2002).

[44] F. Furche and T. van Voorhis, J. Chem. Phys. **122**, 164106 (2005).

[45] F. Furche, J. Chem. Phys. **129**, 114105 (2008).

[46] G. E. Scuseria, T. M. Henderson and D. C. Sorensen, J. Chem. Phys. **129**, 231101 (2008).

[47] B. G. Janesko, T. M. Henderson and G. E. Scuseria, J. Chem. Phys. **130**, 081105 (2009).

[48] J. Toulouse, I. C. Gerber, G. Jansen, A. Savin and J. G. Ángyán, Phys. Rev. Lett. **102**, 096404 (2009).

[49] J. Harl and G. Kresse, Phys. Rev. B **77**, 045136 (2008).

[50] J. Harl and G. Kresse, Phys. Rev. Lett. **103**, 056401 (2009).

[51] D. Lu, Y. Li, D. Rocca and G. Galli, Phys. Rev. Lett. **102**, 206411 (2009).

[52] J. F. Dobson and J. Wang, Phys. Rev. Lett **82**, 2123 (1999).

[53] M. Rohlfing and T. Bredow, Phys. Rev. Lett **101**, 266106 (2008).

[54] X. Ren, P. Rinke and M. Scheffler, Phys. Rev. B **80**, 045402 (2009).

[55] L. Schimka, J. Harl, A. Stroppa, A. Grüneis, M. Marsman, F. Mittendorfer and G. Kresse, Nature Mater. **9**, 741 (2010).

[56] Y. Li, D. Lu, H.-V. Nguyen and G. Galli, J. Phys. Chem. A **114**, 1944 (2010).

[57] X. Ren, A. Tkatchenko, P. Rinke and M. Scheffler, Phys. Rev. Lett. **106**, 153003 (2011).

[58] X. Ren, P. Rinke, C. Joas and M. Scheffler, J Mater. Sci. **47**, 7447 (2012).

[59] D. Lu, H.-V. Nguyen and G. Galli, J. Chem. Phys. **133**, 154110 (2010).

[60] X. Ren, P. Rinke, V. Blum, J. Wieferink, A. Tkatchenko, A. Sanfilippo, K. Reuter and M. Scheffler, New. J. Phys **14**, 053020 (2012).

[61] J. F. Dobson, Quasi-local-density approximation for a van der Waals energy functional, in *Topics in Condensed Matter Physics*, edited by M. P. Das, p. 121, Nova (New York), 1994.

[62] A. Krishtal, K. Vannomeslaeghe, D. Geldof, C. V. Alsenoy and P. Geerlings, Phys. Rev. A **83**, 024501 (2011).

[63] A. Tkatchenko, D. Alfè and K. S. Kim, J. Chem. Theory Comput. **8**, 4317 (2012).

[64] B. M. Axilrod and E. Teller, J. Chem. Phys. **11**, 299 (1943).

[65] T. Helgaker, P. Jørgensen and J. Olsen, *Molecular Electronic Structure Theory* (Wiley, Chichester, 2000).

[66] A. Mayer, Phys. Rev. B **75**, 045407 (2007).

[67] D. W. Oxtoby and W. M. Gelbart, Mol. Phys. **29**, 1569 (1975).

[68] B. T. Thole, Chem. Phys. **59**, 341 (1981).

[69] R. G. Parr and W. Yang, *Density Functional Theory of Atoms and Molecules* (Oxford Science Publications, 1989).

[70] W. Koch and M. C. Holthausen, *A Chemist's Guide to Density Functional Theory* (Wiley-VCH, 2002).

[71] F. L. Hirshfeld, Theor. Chim. Acta **44**, 129 (1977).

[72] W. L. Bade, J. Chem. Phys. **27**, 1280 (1957).

[73] J. Cao and B. J. Berne, J. Chem. Phys. **97**, 8628 (1992).

[74] A. G. Donchev, J. Chem. Phys. **125**, 074713 (2006).

[75] M. W. Cole, D. Velegol, H.-Y. Kim and A. A. Lucas, Mol. Simul. **35**, 849 (2009).

[76] H. Berthoumieux and A. C. Maggs, Europhys. Lett. **91**, 56006 (2010).

[77] A. Tkatchenko, A. Ambrosetti and R. A. DiStasio, Jr., arXiv:1210.8343 (2012).

[78] T. W. Whitfield and G. J. Martyna, Chem. Phys. Lett. **424**, 409 (2006).

[79] A. Jones, A. Thompson, J. Crain, M. H. Müser and G. J. Martyna, Phys. Rev. B **79**, 144119 (2009).

[80] P. Jurecka, J. Sponer, J. Cerny and P. Hobza, Phys. Chem. Chem. Phys. **8**, 1985 (2006).

[81] T. Takatani, E. G. Hohenstein, M. Malagoli, M. S. Marshall and C. D. Sherrill, J. Chem. Phys. **132**, 144104 (2010).

[82] J. P. Perdew, K. Burke and M. Ernzerhof, Phys. Rev. Lett. **77**, 3865 (1996).

[83] J. P. Perdew, M. Ernzerhof and K. Burke, J. Chem. Phys. **105**, 9982 (1996).

[84] C. Adamo and V. Barone, J. Chem. Phys. **110**, 6158 (1999).

[85] V. V. Gobre *et al.*, in preparation.

[86] R.-F. Liu, J. G. Angyan and J. F. Dobson, J. Chem. Phys. **134**, 114106 (2011).

[87] J. R. Hammond, M. Valiev, W. A. de Jong and K. Kowalski, J. Phys. Chem. A **111**, 5492 (2007).

[88] J. R. Hammond, K. Kowalski and W. A. de Jong, J. Chem. Phys. **127**, 144105 (2007).

[89] S. Botti, A. Castro, X. Andrade, A. Rubio and M. A. L. Marques, Phys. Rev. B **78**, 035333 (2008).

[90] A. Kumar, M. Kumar and W. J. Meath, Chem. Phys. **286**, 227 (2003).

[91] V. Blum, R. Gehrke, F. Hanke, P. Havu, V. Havu, X. Ren, K. Reuter and M. Scheffler, Comp. Phys. Commun. **180**, 2175 (2009).

[92] O. A. Vydrov and T. Van Voorhis, J. Chem. Phys. **133**, 244103 (2010).

[93] J. Rezac, K. E. Riley and P. Hobza, J. Chem. Theory Comput. **7**, 2427 (2011).

[94] W. Chin, F. Piuzzi, I. Dimicoli and M. Mons, Phys. Chem. Chem. Phys. **8**, 1033 (2006).

[95] J. P. Simons, Mol. Phys. **107**, 2435 (2009).

[96] F. Bierau, P. Kupser, G. Meijer and G. von Helden, Phys. Rev. Lett. **105**, 133402 (2010).

[97] M. P. Gaigeot, Phys. Chem. Chem. Phys. **12**, 3336 (2010).

[98] J. A. Stearns, C. Seaiby, O. V. Boyarkin and T. R. Rizzo, Phys. Chem. Chem. Phys. **11**, 125 (2009).

[99] M. Rossi, V. Blum, P. Kupser, G. von Helden, F. Bierau, K. Pagel, G. Meijer and M. Scheffler, J. Phys. Chem. Lett. **1**, 3465 (2010).

[100] R. L. Baldwin, J. Mol. Biol. **371**, 283 (2007).

[101] A. Tkatchenko, M. Rossi, V. Blum, J. Ireta and M. Scheffler, Phys. Rev. Lett. **106**, 118102 (2011).

[102] R. A. DiStasio Jr., Y. Jung and M. Head-Gordon, J. Chem. Theory Comput. **1**, 862 (2005).

[103] R. A. DiStasio Jr., R. P. Steele, Y. M. Rhee, Y. Shao and M. Head-Gordon, J. Comp. Chem. **28**, 839 (2007).

[104] K. N. Trueblood, H.-B. Bürgi, H. Burzlaff, J. D. Dunitz, C. M. Gramaccioli, H. H. Schulz, U. Shmueli and S. C. Abrahams, Acta Crys. A **52**, 770 (1996).

[105] A. Sygula, F. R. Fronczek, R. Sygula, P. W. Rabideau and M. M. Olmstead, J. Am. Chem. Soc. **129**, 3842 (2007).

[106] J. Bernstein, *Polymorphism in Molecular Crystals* (Oxford University Press, USA (New York), 2002).

[107] S. L. Price, Phys. Chem. Chem. Phys. **10**, 1996 (2008).

[108] D. A. Bardwell *et al.*, Acta. Cryst. B **67**, 535 (2011).

[109] G. J. O. Beran and K. Nanda, J. Phys. Chem. Lett. **1**, 3480 (2010).

[110] S. Wen, K. Nanda, Y. Huang and G. Beran, Phys. Chem. Chem. Phys. **14**, 7578 (2012).

[111] K. Hongo, M. A. Watson, R. S. Sanchez-Carrera, T. Iitaka and A. Aspuru-Guzik, J. Phys. Chem. Lett. **1**, 1789 (2010).

[112] B. Schatschneider, J.-J. Liang, A. M. Reilly, N. Marom, G.-X. Zhang and A. Tkatchenko, arXiv:1211.1683.

[113] M. V. Roux, M. Temprado, J. S. Chickos and Y. Nagano, J. Phys. Chem. Ref. Data **37**, 1855 (2008).

[114] A. M. Reilly and A. Tkatchenko, in preparation.

[115] N. Marom, R. A. DiStasio, Jr., V. Atalla, S. Levchenko, J. R. Chelikowsky, L. Leiserowitz and A. Tkatchenko, arXiv:1210.5636.

[116] J. J. Rehr, E. Zaremba and W. Kohn, Phys. Rev. B **12**, 2062 (1975).